

Analysis of a Summertime PM_{2.5} and Haze Episode in the Mid-Atlantic Region

L.-W. Antony Chen and Judith C. Chow

Atmospheric Science Division, Desert Research Institute, Reno, Nevada

Bruce G. Doddridge and Russell R. Dickerson

Department of Meteorology, University of Maryland, College Park, Maryland

William F. Ryan

Department of Meteorology, Pennsylvania State University, University Park, Pennsylvania

Peter K. Mueller

TropoChem, Palo Alto, California

ABSTRACT

Observations of the mass and chemical composition of particles less than 2.5 μm in aerodynamic diameter (PM_{2.5}), light extinction, and meteorology in the urban Baltimore-Washington corridor during July 1999 and July 2000 are presented and analyzed to study summertime haze formation in the mid-Atlantic region. The mass fraction of ammoniated sulfate (SO₄²⁻) and carbonaceous material in PM_{2.5} were each ~50% for cleaner air (PM_{2.5} < 10 $\mu\text{g}/\text{m}^3$) but changed to ~60% and ~20%, respectively, for more polluted air (PM_{2.5} > 30 $\mu\text{g}/\text{m}^3$). This signifies the role of SO₄²⁻ in haze formation. Comparisons of data from this study with the Interagency Monitoring of Protected Visual Environments network suggest that SO₄²⁻ is more regional than carbonaceous material and originates in part from upwind source regions. The light extinction coefficient is well correlated to PM_{2.5} mass plus water associated with inorganic salt, leading to a mass extinction efficiency of $7.6 \pm 1.7 \text{ m}^2/\text{g}$ for hydrated aerosol. The most serious haze episode occurring between July 15 and

19, 1999, was characterized by westerly transport and recirculation slowing removal of pollutants. At the peak of this episode, 1-hr PM_{2.5} concentration reached ~45 $\mu\text{g}/\text{m}^3$, visual range dropped to ~5 km, and aerosol water likely contributed to ~40% of the light extinction coefficient.

INTRODUCTION

Haze pollution has been studied intensively during the last decade for its impact on our visual environment, climate, and public health. Haze is caused by small particles scattering/absorbing visible radiation in the atmosphere.¹ In the United States, the atmospheric extinction (scattering plus absorbing) coefficient is monitored at all major airports through the Automated Surface Observing System (ASOS; see www.nws.noaa.gov/asos) and is used to calculate effective visual range,² a crucial parameter for flight safety. Since 1987, the Interagency Monitoring of Protected Visual Environments (IMPROVE) network has been measuring the temporal and spatial trends of visibility in the U.S. National Parks.^{3,4} IMPROVE results suggest that haze is often regional in nature and is not restricted to urban or industrialized areas. Regional haze events can occur in all seasons. Understanding the link between local and regional emissions and the formation of haze is critical to effective air quality regulation.

A hazy condition is distinguished by low visibility. Visibility is a measure of the human eye's ability to distinguish an object from the surrounding background. This ability is restricted by suspended materials that attenuate the light emitted or reflected by the object.

IMPLICATIONS

This article studies summertime PM_{2.5} and haze in the mid-Atlantic region. Temporal and spatial variations in the chemical composition of PM_{2.5} and its relation to changes in the light extinction coefficient are investigated. Visibility reduction is an outcome of rapid SO₄²⁻ accumulation in a humid atmosphere. Sulfate and haze accumulate on the regional scale. Data from continuous monitoring and a thermodynamic model suggest that both local and regional emissions and meteorology contribute to the occurrence of a severe haze episode.

According to the Koschmeider equation,⁵ visibility can be estimated from the atmospheric extinction coefficient:

$$\text{Visibility} \sim \frac{3.912}{b_{\text{ext}}} \quad (1)$$

The scattering by air molecules (Rayleigh scattering) is $\sim 13 \text{ Mm}^{-1}$ at 520 nm at sea level. Rayleigh scattering limits the visibility in the cleanest atmosphere to ~ 300 km. Over the Earth's continents, scattering and absorption by fine-mode particles, with size of the same order as the wavelength of visible radiation, contribute to most of the observed light extinction. The IMPROVE network uses data on chemically speciated particles less than $2.5 \mu\text{m}$ in aerodynamic diameter ($\text{PM}_{2.5}$) to reconstruct the extinction coefficient and achieves a reasonable agreement with the measured values.⁶ However, $\text{PM}_{2.5}$ mass and chemical composition can vary significantly from day to day. The IMPROVE data, based on every-third-day sampling, are not sufficient for resolving the evolution of $\text{PM}_{2.5}$ /haze episodes.

In the U.S. mid-Atlantic region, haze is frequently reported during the summer months.^{7,8} This region is one of the most populated in the country. Industries and utility generation in the cities, motor vehicle emissions, and residential cooking/heating all contribute to the ambient fine aerosol mass. In addition, previous research has shown that emissions from the industrialized U.S. Midwest can be transported downwind to the mid-Atlantic region.^{9,10} The Maryland Aerosol Research and Characterization (MARCH)-Atlantic study set up a sampling site at Fort Meade (FME), MD (39.10°N , 76.74°W ; elevation 46 m mean sea level), almost in the middle of the Baltimore-Washington (B-W) corridor. The FME site is one of the U.S. Environmental Protection Agency (EPA) Photochemical Assessment and Monitoring Stations (PAMS) with continuous monitoring of ozone (O_3), reactive nitrogen species (NO_x), and volatile organic compounds (VOCs) in place. For this study, additional instruments were installed to determine the $\text{PM}_{2.5}$ mass and chemical composition, and concentrations of precursor gases such as nitric acid (HNO_3) and ammonia (NH_3). Measurements of the key pollution tracers carbon monoxide (CO), which is nearly conserved on synoptic time scales, and sulfur dioxide (SO_2), a precursor gas of sulfate (SO_4^{2-}), began in June 1999 and October 1999, respectively. The FME site is equipped with a radar profiler (Radian 915 mHz, Radian Corp.) that continuously acquires wind speed and direction up to 4 km above ground level (AGL). Atmospheric extinction coefficients were obtained through an ASOS station at the Baltimore Washington International (BWI) Airport, ~ 15 km north of FME.

In this paper, we present the observations at FME and BWI during two summer months, July 1999 and July 2000. July 1999 was unusually warm and dry in the mid-Atlantic region. Daily maximum temperature on 26 of 33 sampling days was above 31°C (the 30-yr norm) at BWI while precipitation was less than 50% of the climate norm. The hot and dry conditions were conducive to O_3 formation, and the Baltimore area recorded six Code Red (1-hr $\text{O}_3 > 124$ ppbv; unhealthy) and 11 Code Orange (1-hr O_3 between 105 and 124 ppbv; unhealthy for sensitive groups) days in the month. These O_3 episodes were usually accompanied by severe visibility reduction (see www.meto.umd.edu/~ryan/summary99.htm).

In contrast, only three out of 33 sampling days in July 2000 experienced maximum temperature at or above 31°C , and precipitation was nearly twice the climate norm. No Code Red days occurred in this month. Temporal and spatial variations of $\text{PM}_{2.5}$ mass and chemical composition as well as visible light extinction in the two months are examined. These results, along with radar profiler observations and air parcel back trajectory analyses, are used to study a severe haze episode in July 1999. The goal is to understand how various factors contribute to haze formation.

TECHNICAL APPROACHES

The location of FME, relative to the IMPROVE network, is shown in Figure 1. The environment and configuration of the sampling site are described in Chen et al.^{11,12} and Chen.¹³ Although within the B-W corridor, this site, located on a military base, is less urban than the EPA Baltimore supersite (see www.chem.umd.edu/supersite/intro.htm) and the IMPROVE site at Washington, DC.

Twenty-four-hour $\text{PM}_{2.5}$ mass concentrations were acquired daily through a sequential filter sampler (SFS)^{14,15} modified by the Desert Research Institute (DRI) and also every third day through a Federal Reference

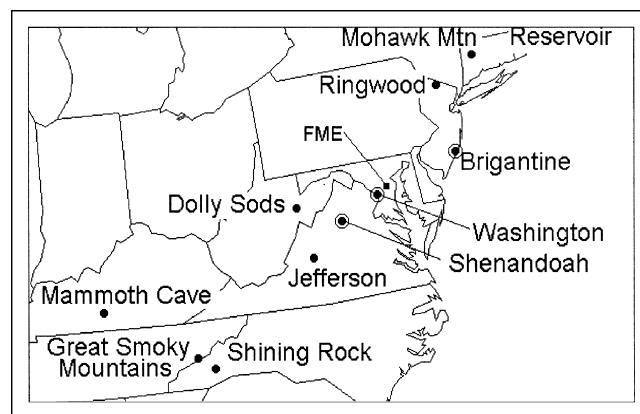


Figure 1. Locations of FME and IMPROVE network sites in the mid-Atlantic region. The three sites circled are chosen for comparisons with FME in this study.

Method (FRM) sampler (Anderson RAAS 2.5 Model 300). Both SFS and FRM are gravimetric methods, utilizing Teflon filters and weighing the filters at $\sim 30\%$ relative humidity (RH) before and after sampling to determine the aerosol mass loading. A $PM_{2.5}$ cyclone inlet (Bendix/Sensidyne Model 240 cyclone) is used for the SFS, while the FRM sampler adopts an impactor inlet. Hourly $PM_{2.5}$ mass concentration was measured continuously using a tapered element oscillating microbalance (TEOM; Series 1400a, Rupprecht & Patashnick Co.) equipped with a $PM_{2.5}$ sharp-cut cyclone inlet. The TEOM is an inertial-method instrument that draws ambient air through a filter at a constant flow rate (3 L/m), continuously weighing the filter and calculating near real-time mass concentration. To evaporate water associated with aerosol, the sample air was preheated to 50°C before being drawn into the instrument.

Exposed Teflon filters collected from the SFS were used to determine ~ 40 elements (from sodium [Na] to uranium, by X-ray fluorescence) besides aerosol mass. The second channel of the SFS contained a quartz filter followed by a sodium chloride (NaCl)-impregnated cellulose backup filter. The quartz filter was used to determine the concentration of water-soluble ions (chlorine [Cl^-], nitrate [NO_3^-], and SO_4^{2-} by ion chromatography; ammonium [NH_4^+] by colorimetry; Na^+ and potassium [K^+] by atomic absorption spectrometry), while the cellulose filter was used for capturing NO_3^- volatilized from the front quartz filter. Nitrate reported is the sum of NO_3^- from front and backup filters. Carbonaceous material was also determined at 24-hr resolution using another SFS in which quartz filters were installed to sample the air. The thermal optical reflectance method (TOR)¹⁶ was applied to measure elemental carbon (EC) and organic carbon (OC) on the front quartz filters based on the IMPROVE thermal protocol.^{16,17}

Twenty-four-hour average gaseous HNO_3 and NH_3 concentrations were obtained using two sequential gas samplers (SGSs) designed by DRI.¹⁵ Both channels of SGSs contained a quartz filter followed by a backup cellulose filter, but only one of them contained a denuder upstream of the filters that can remove HNO_3 or NH_3 . Total nitrate (T- NO_3^- : $\text{HNO}_3 + \text{NO}_3^-$) or total ammonium (T- NH_4^+ : $\text{NH}_3 + \text{NH}_4^+$) was collected by one channel, while only particulate NO_3^- or NH_4^+ was collected by the other channel. The HNO_3 or NH_3 concentration was then determined from the difference between the two channels.

Every single measurement from SFS or SGS contains uncertainties from four origins: sample volume, analytical noise, deposition homogeneity, and field blank concentration. The uncertainty from each origin is estimated (e.g., by flow rate performance test and replicate analysis) and propagated to calculate the measurement precision.

The overall uncertainty associated with each ambient datum is then reported; it is typically within $\pm 10\%$ for a measured value that exceeds 10 times lower detection limits.^{14,15,18} For a total of 66 sampling days in July 1999 and July 2000, all of the mass, SO_4^{2-} , NH_4^+ , OC, and EC measurements have uncertainties at or below 10%. The errors in the FRM and TEOM measurements are not as well tested. They, however, can be evaluated through intercomparisons with the SFS mass data.

One-hour average CO was measured continuously throughout the period using a commercial instrument (Thermo Environment Instruments Model 48) modified to improve sensitivity and selectivity.^{19,20} The detection limit for CO is ~ 10 ppbv and analytical uncertainties $< 10\%$ are expected (95% confidence for a 60-min integration) for CO concentration ranging from 100 to 2000 ppbv. The instrument was calibrated every three months using standards traceable to National Institute of Standard and Technology for quality assurance.

The ASOS at BWI employs a Belfort Model 6220 forward scatter visibility meter (Belfort Instrument) to measure the clarity of the air. The system cants the transmitter and receiver at a small angle, preventing direct light from striking the receiver. ASOS projects light from a Xenon flash lamp (visible spectrum 515 ± 6 nm) in a cone-shaped beam. The receiver measures only the light scattered forward. The b_{ext} is assumed as being dominated by forward scattering. The detection limit for 1-min average b_{ext} is $\sim 50 \text{ Mm}^{-1}$, which corresponds to a visual range ~ 80 km. According to the manufacturer, measurement uncertainty is within 10% for b_{ext} from 10^2 to 10^6 Mm^{-1} (visual range 5 m to 50 km).

Air parcel back trajectories are used to study atmospheric transport and potential source regions linked to each pollution episode. As part of the MARCH-Atlantic study, back trajectories were calculated for every sampling day using the Hybrid Single-Particle Lagrangian Integrated Trajectories (HY-SPLIT) model.^{21,22} HY-SPLIT was configured using wind fields generated by the National Centers for Environmental Prediction (NCEP) Eta Data Assimilation System (EDAS) and analyzed over a domain encompassing the continental United States (20°N – 55°N , 60°W – 130°W ; see www.arl.noaa.gov/ready/hysplit4.html). Draxler²¹ reported a potential error of 20–30% of total travel distance when comparing HY-SPLIT calculated trajectories with tracer plumes. Because the model terrain is smoother than the actual terrain, calculated trajectories near the surface in and near areas of complex terrain are less accurate than trajectories at higher levels. This is primarily caused by difficulties in resolving small-scale frictional and turbulent effects. As a result, back trajectories are calculated at ~ 1000 m AGL or approximately in the middle of the afternoon well-mixed layer.

PM_{2.5} MASS AND CHEMICAL COMPOSITION

Figures 2a and b show the time series of PM_{2.5} mass and speciation concentration measured by SFSs in July 1999 and 2000, respectively. The SFS mass data are compared with concurrent measurements of FRM and TEOM in Figure 3. The correlation between SFS and FRM is high ($r^2 \sim 0.97$) with an FRM/SFS slope ~ 1.1 . This agrees with Watson and Chow,²³ who reported a $\sim 10\%$ positive bias in mass measurements by the same type of FRM instrument with respect to the DRI SFS. Because the FRM and SFS are both gravimetric methods and adopt similar sampling substrate and procedure, the 10% deviation could result from using different size-selective inlets (impactor vs. cyclone). Taking into account the 5–10% analytical uncertainty existing in the SFS mass concentration (Figure 3), FRM and SFS can be considered in good agreement.

Twenty-four-hour average TEOM is also well correlated to SFS ($r^2 \sim 0.91$), but a significant negative bias (TEOM less than SFS and FRM by $>10\%$; Figure 3) appears on low PM_{2.5} days. This deficit is likely caused by the loss of volatile NO₃⁻ and organics when sample air is pre-heated to 50 °C.²⁴ In summer, low PM_{2.5} conditions often

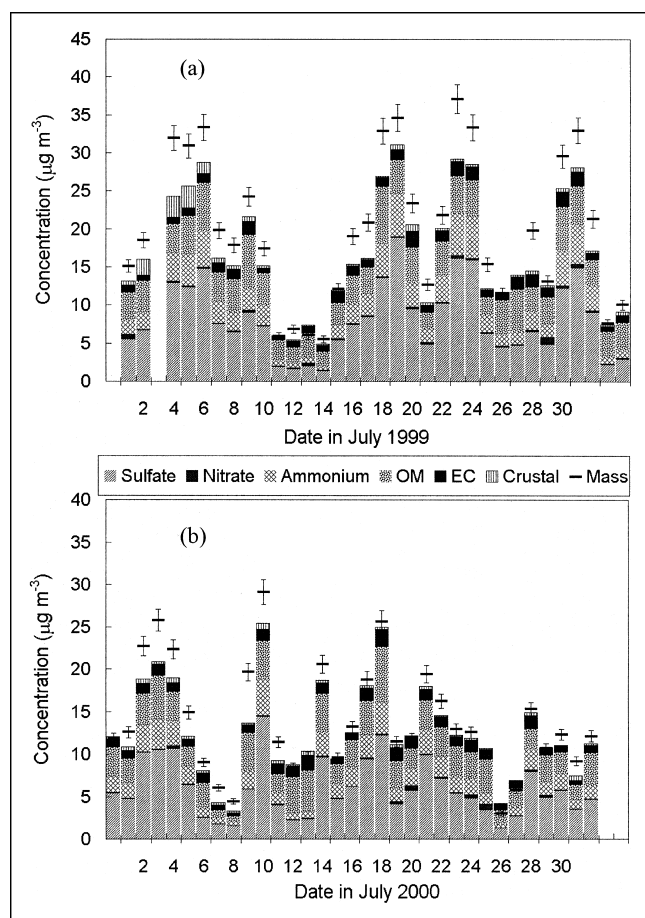


Figure 2. Time series of PM_{2.5} gravimetric mass and reconstructed mass measured by DRI SFSs at FME during (a) July 1999 and (b) July 2000. Analytical uncertainty of the gravimetric mass is shown.

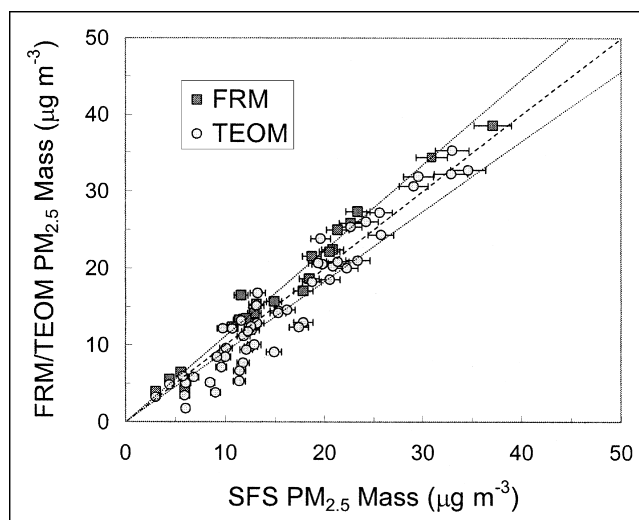


Figure 3. Comparisons of 24-hr PM_{2.5} mass measured by SFS, FRM, and TEOM at FME during July 1999 and 2000. The dashed line indicates the 1:1 and $\pm 10\%$ lines. Analytical uncertainty of the SFS mass is shown.

occur at cooler ambient temperatures. The lower the ambient temperature, the more material could be lost as sample stream is heated. The comparison in Figure 3 suggests that TEOM data are reliable on high PM_{2.5} days and adequate for studying PM_{2.5}/haze episodes.

Major species contributing to PM_{2.5} mass include SO₄²⁻, NO₃⁻, NH₄⁺, OC, EC, and crustal material. Organic matter (OM) is determined from $1.4 \times \text{OC}$ to account for oxygen (O), hydrogen (H), and nitrogen (N) atoms in organics.²⁵ The mass of crustal material (CM) is estimated from aluminum (Al), silicon (Si), calcium (Ca), and iron (Fe) (i.e., $1.89 \times \text{Al} + 2.14 \times \text{Si} + 1.4 \times \text{Ca} + 1.43 \times \text{Fe}$).¹⁷ The analytical uncertainties of CM were all below 10% in this study. Aerosol reconstructed mass calculated by summing SO₄²⁻, NO₃⁻, NH₄⁺, OM, EC, and CM agreed closely with the gravimetric mass from SFS with $r^2 \sim 0.97$ and slope ~ 0.9 . On average, the six major species explained more than 80% of the PM_{2.5} mass.

During the two months, particulate NO₃⁻ was generally negligible because gaseous HNO₃ is favored under warm temperature conditions.²⁶ CM concentration remained low (~ 1 –3% of the PM_{2.5} mass) except between July 2 and July 6, 1999, when it exceeded 10 times the monthly mean. NH₄⁺ was strongly correlated with SO₄²⁻ ($r^2 \sim 0.97$) with the NH₄⁺/SO₄²⁻ molar ratio of ~ 1.7 . To maintain the ionic balance, the majority of inorganic aerosol was likely an acidic mixture of ammonium sulfate [(NH₄)₂SO₄] and NH₄HSO₄. Overall, ammoniated sulfate (NH₄⁺ + SO₄²⁻) accounted for more than half ($52 \pm 9\%$) of the PM_{2.5} mass, followed by OM ($25 \pm 11\%$) and EC ($8 \pm 4\%$).

In July 1999, there were four episodes with a maximum 24-hr PM_{2.5} concentration of more than 30 µg/m³, but only one in July 2000 was close to this level (July

9–11). Hot smoggy conditions in the summer of 1999 led to high O_3 and H_2O_2 concentrations, accelerating secondary aerosol formation, while the lack of precipitation slowed deposition rates. The mass fraction of ammoniated sulfate in $PM_{2.5}$ increased with $PM_{2.5}$ mass and reached $\sim 60\%$ when $PM_{2.5}$ was $>30 \mu\text{g}/\text{m}^3$. The mass fraction of carbonaceous material (EC + OM), however, decreased to $\sim 20\%$ (Figure 4). Although the concentration of carbonaceous material was relatively constant, the high $PM_{2.5}$ episodes were largely driven by elevated ammoniated sulfate levels.

The $PM_{2.5}$ reconstructed mass was usually less than the gravimetric mass, and on high $PM_{2.5}$ days the difference could be significantly greater than the 10% analytical uncertainty of gravimetric mass (Figures 2a-b). Possible sources of the deficit include underestimations of OM and CM and certain unidentified species. Turpin and Lim²⁷ suggested that the OM/OC ratio in an urban environment could be higher than 1.4, providing a plausible explanation for the “missing” mass. However, the correlation (r) of the mass deficit with SO_4^{2-} is high at 0.73 (only 0.38 with OM). Malm et al.³ and Rees et al.²⁸ suggested that water associated with inorganic salts could account for part of the unidentified mass. Though the $PM_{2.5}$ gravimetric mass in this study was determined at $\sim 30\%$ RH, well below the deliquescence relative humidity (DRH, the RH at which a species starts to take up water vapor) of $(NH_4)_2SO_4$ and ammonium nitrate, water associated with SO_4^{2-} or NO_3^- might not evaporate completely because of hysteresis effects.²⁹ In ambient conditions, RH is usually higher than 30% so that water associated with SO_4^{2-} is expected to be even more significant.

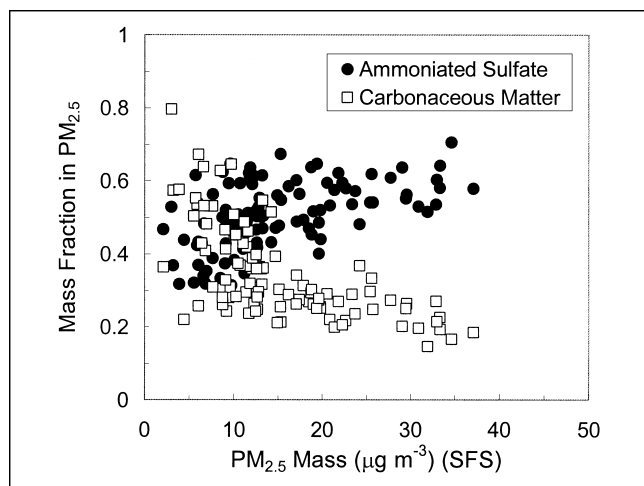


Figure 4. Mass fraction of ammoniated sulfate and carbonaceous material in $PM_{2.5}$ vs. $PM_{2.5}$ gravimetric mass. Data were acquired at FME during July 1999 and July 2000.

SPATIAL VARIATION OF $PM_{2.5}$ SPECIES

The IMPROVE network operates ~ 150 air/visibility monitoring sites in the National Parks and Wilderness Areas across the United States. Twenty-four-hour average chemically speciated $PM_{2.5}$ data are acquired twice a week at each site.^{3,4} Sulfur and other elements such as Al, Si, Ca, and Fe are measured on Teflon filters by particle-induced X-ray emission or X-ray fluorescence at the University of California, Davis. SO_4^{2-} and NO_3^- ions are analyzed on nylon filters by ion chromatography. EC and OC are analyzed by TOR at DRI. In this study, SO_4^{2-} , EC, OM, and CM at three IMPROVE sites, Washington, Shenandoah, and Brigantine (Figure 1), are compared with concurrent measurements at FME to determine their spatial variations in the mid-Atlantic region. EC and OM were determined using the same facilities/procedures and are comparable between sites. For SO_4^{2-} and CM, analytical uncertainties $<10\%$ for each single measurement were reported by both DRI and the IMPROVE network.

The Washington site (WASH, 38.88 °N, 77.05 °W; elevation 10 m mean sea level), located in downtown Washington, DC, is one of a few urban sites in the IMPROVE network. WASH is <20 km south of FME. Because the WASH and FME sites are closely located in the B-W corridor, their data can be compared to examine the homogeneity of pollutant distribution inside the urban corridor. The Shenandoah site (SHEN, 38.52 °N, 78.44 °W; elevation 1097 m mean sea level) is rural, located at Big Meadows, Shenandoah National Park, west-southwest and generally upwind of FME. This site is at the eastern boundary of the Appalachian Mountains and is less influenced by surface sources because of its elevation.^{30–32} The Brigantine site (BRIG, 39.47 °N, 74.45 °W; elevation 5 m mean sea level) is also rural, located in the Brigantine National Wildlife Reserve, generally downwind of FME and several kilometers from the Atlantic Ocean. Both SHEN and BRIG are ~ 200 km away from FME and WASH. Observations at SHEN and BRIG, when compared with WASH and FME data, may resolve contributions from the B-W corridor.

Sulfate, EC, OM, and CM concentrations at FME in July 1999 and 2000 are plotted against concurrent measurements at SHEN, WASH, and BRIG in Figures 5a-d. (For a sampling frequency approximately twice a week, the number of samples is probably equal to the number of independent observations, assuming the autocorrelation induced by coherence on synoptic scales on roughly 3 days during summer.) The FME and WASH data generally show good correspondences in SO_4^{2-} , EC, and OM concentrations ($r^2 \sim 0.7–0.9$), three major components in $PM_{2.5}$. The $PM_{2.5}$ mass and chemical composition determined at FME seem not to be seriously contaminated

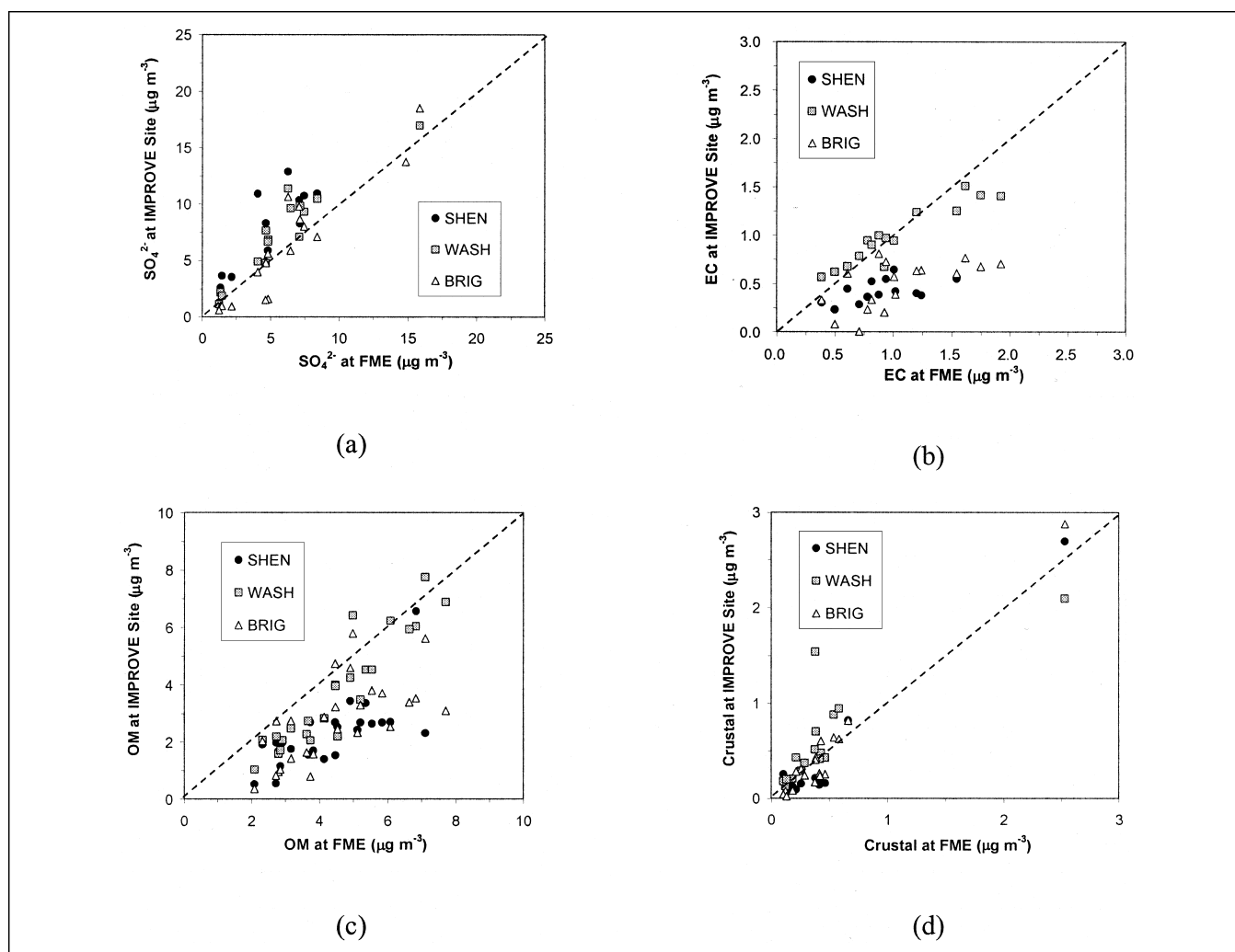


Figure 5. Scatter plots of 24-hr mean (a) SO_4^{2-} , (b) EC, (c) OM, (d) CM concentration at FME vs. concurrent measurements at three IMPROVE sites, SHEN, WASH, and BRIG, during July 1999 and 2000. The dashed line indicates 1:1 correspondence.

by nearby sources and therefore can be considered representative for the urban corridor.

For SO_4^{2-} , good correlations are found not only between FME and WASH but also between FME and the other two IMPROVE sites ($r^2 \sim 0.7\text{--}0.9$). On 12 of 13 days when concurrent measurements at the four sites are available, the highest SO_4^{2-} concentration appeared at the upwind high elevation site, SHEN. These observations suggest that SO_4^{2-} is widespread over a region >400 km in diameter and could extend vertically from the surface to the top of mixing layer.

Chen et al.¹² and Stehr et al.¹⁰ presented HY-SPLIT air parcel back trajectories associated with high SO_4^{2-} and SO_2 episodes, respectively, in the mid-Atlantic region and suggested strong contributions of sulfur emissions from the U.S. Midwest. EPA emissions analyses³³ show that coal-fired electric utilities in the Ohio River Valley and surrounding areas emit a high proportion of regional-scale SO_2 emissions. The SO_2 emitted from these sources is mixed upward in the planetary boundary layer (PBL),

converted to SO_4^{2-} through cloud processes and may be carried over the Appalachian Mountains by prevailing winds. Transport can be quite rapid above the nocturnal boundary layer (NBL) in the overnight hours, and the transported $\text{SO}_2/\text{SO}_4^{2-}$ is then mixed downward the following day, at great distances from its source, by the evolving PBL. Chen et al.¹¹ showed a midday peak in the SO_2 diurnal profile that supported downward mixing of SO_2 from aloft in the early afternoon. This conceptual model of transport explains the observed spatial homogeneity of SO_4^{2-} as well as the regional nature of haze in the mid-Atlantic region.

The EC concentrations at FME and WASH are well correlated ($r^2 \sim 0.88$) but are generally higher than at SHEN and BRIG. The correlations of FME EC with SHEN EC and BRIG EC are lower at $r^2 \sim 0.38$ and $r^2 \sim 0.29$, respectively. In contrast to SO_4^{2-} , EC appears to have a narrower spatial distribution centered along the B-W corridor. Chen et al.¹¹ found good correlations between EC and CO at FME, suggesting the influence of on-road

mobile emissions on both EC and CO concentrations. The observed spatial distribution supports different source regions for SO_4^{2-} and EC. Combining factor and ensemble back trajectory analyses, Chen et al.¹² attribute >60% of EC at FME to mobile sources in the corridor and >80% of SO_4^{2-} to sources from the Midwest.

The spatial pattern of OM is similar to that of EC except showing a stronger correlation between the FME and SHEN OM concentration ($r^2 \sim 0.62$, intermediate between SO_4^{2-} and EC). Though the mobile emissions in the urban corridor produce substantial OM in addition to EC, there are also regional OM sources, such as biogenic emissions and secondary OM formed in the atmosphere from semi-volatile organic compounds.

The CM concentration generally stays below $1 \mu\text{g}/\text{m}^3$, with the exception of increased concentrations on July 3, 1999. Excluding this outlier, CM at FME is moderately correlated with that at WASH, SHEN, and BRIG at $r^2 \sim 0.5$. Though dust generated by traffic, construction work, and other anthropogenic activities in the corridor could be substantial, they are mostly coarse-mode particles. The occasional elevated fine-mode crustal concentration is likely dominated by more distant sources. A significant crustal episode occurred between July 2 and 6, 1999, with concentrations of crustal material reaching $\sim 3 \mu\text{g}/\text{m}^3$, and accounted for as much as 10% of the $\text{PM}_{2.5}$ mass (Figure 2). Prospero³⁴ suggested that intercontinental transport of the Saharan dust could impact air quality in the southeastern United States. The HY-SPLIT back trajectory initiated at midday July 3, 1999, does trace the air parcel above FME back to northeastern Africa in ~ 20 days.³⁵

PM_{2.5} MASS AND VISIBILITY

Ammoniated sulfate, the most abundant $\text{PM}_{2.5}$ species at FME, is hygroscopic, and fine aerosol mass at ambient RH can be greater than measured dry mass because of aerosol water content. Theoretically, ammoniated sulfate begins to take up water vapor once RH exceeds DRH. The increase in water content changes both the aerosol scattering cross section and the light extinction efficiency. To relate the measured dry $\text{PM}_{2.5}$ concentration to b_{ext} we need to estimate aerosol water content based on known temperature, RH, and aerosol composition. A chemical thermodynamic model, ISORROPIA, was used to study the aqueous/gaseous partitioning of H_2O by assuming thermodynamic equilibrium.

ISORROPIA is a bulk aerosol model designed for a $\text{Na}^+ \text{-NH}_4^+ \text{-Cl}^- \text{-SO}_4^{2-} \text{-NO}_3^- \text{-H}_2\text{O}$ system.^{36,37} Aerosol is assumed to be internally mixed, meaning that all particles of the same size have the same chemical composition. ISORROPIA considers all possible reactions in gaseous, aqueous, and solid phases and the mutual deliquescence

relative humidity of a salt mixture.³⁸ The model can handle either "forward" or "reverse" approaches. In the forward approach, the inputs include concentration of Na^+ , Cl^- , T- NH_4^+ ($\text{NH}_4^+ + \text{NH}_3$), T- NO_3^- ($\text{NO}_3^- + \text{HNO}_3$), and SO_4^{2-} ; the model calculates the abundance of NO_3^- , NH_4^+ , and water (H_2O) in condensed (aqueous + solid) phase and HNO_3 and NH_3 in gaseous phase. In the reverse approach, inputs are aerosol-phase Na^+ , Cl^- , NH_4^+ , NO_3^- , and SO_4^{2-} ; gaseous NH_3 and HNO_3 are calculated by the model. This study adopted the forward approach and assumed that Cl^- and Na^+ were negligible. Daily mean temperature and RH were used in the model because speciated $\text{PM}_{2.5}$ data are limited to 24-hr resolution. The equilibrium constants, K_{eq} , vary near linearly with temperature in the range of a typical day but can be nonlinear with respect to RH.³⁹ In the high ambient temperatures of summer, the model usually predicts an excess of HNO_3 over NO_3^- . Chen¹³ showed that the calculated gas/aerosol partitioning of T- NO_3^- and T- NH_4^+ , based on 24-hr mean temperature and RH, generally agree with measurements within the range of analytical uncertainties. Errors introduced by using 24-hr average temperature and RH are not significant.

Figure 6 compares 24-hr average b_{ext} acquired from BWI with reconstructed $\text{PM}_{2.5}$ mass (just SO_4^{2-} , NO_3^- , NH_4^+ , OM, EC, and CM with no H_2O content) at FME. To exclude poor visibility conditions caused by fog or precipitation rather than aerosol, data from dates with mean RH >87% were not used. The correlation (r^2) between the reconstructed $\text{PM}_{2.5}$ mass and b_{ext} is ~ 0.4 . Outlier points tend to appear on the haziest days ($b_{\text{ext}} > 300 \text{ Mm}^{-1}$). When including H_2O associated with SO_4^{2-} , NO_3^- , and NH_4^+ (estimated by ISORROPIA), the correlation (r^2) is improved to ~ 0.6 (Figure 6). Apportioning b_{ext} to the six

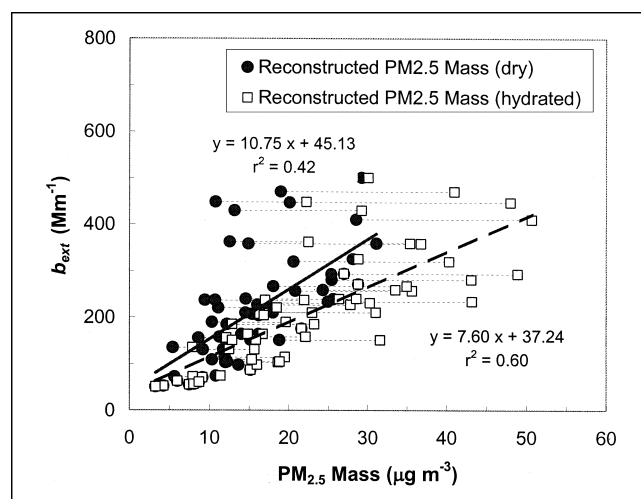


Figure 6. Scatter plot of 24-hr extinction coefficient (b_{ext}) at BWI vs. 24-hr $\text{PM}_{2.5}$ mass concentration with/without water at FME for July 1999 and 2000. Aerosol water content was estimated by ISORROPIA.

major species through multiple linear regression does not further improve the correlation. The spatial variation of b_{ext} and $\text{PM}_{2.5}$ concentration between BWI and FME and unknown hygroscopicity of carbonaceous aerosol may have prevented a more strict correspondence between the observed b_{ext} and ambient $\text{PM}_{2.5}$.

The $b_{\text{ext}}/\text{mass}$ slope in Figure 6 yields an aerosol mass extinction efficiency (at 95% confidence level) of $7.6 \pm 1.7 \text{ m}^2/\text{g}$ for hydrated aerosol and $10.8 \pm 3.4 \text{ m}^2/\text{g}$ if the H_2O is neglected. On average, H_2O is responsible for approximately one-third of the b_{ext} . Hegg et al.⁴⁰ suggested a mass scattering efficiency (at 550 nm) of $4 \pm 1.1 \text{ m}^2/\text{g}$ for carbon species and $2.7 \pm 1.3 \text{ m}^2/\text{g}$ for dry ammoniated sulfate (at ~30% RH) in a haze plume traveling off the mid-Atlantic coast. Absorption was suggested to contribute as much as 25% to the total dry extinction. The overall mass extinction efficiency in Hegg et al.⁴⁰ is lower than $7 \text{ m}^2/\text{g}$ but is within a factor of 2. For particles ~1 μm in diameter, H_2O can have a higher scattering efficiency than SO_4^{2-} and carbon,⁴¹ and that likely increases the overall extinction efficiency of hydrated aerosols in ambient atmosphere. Another possibility for the higher extinction efficiency in this study results from using wavelengths shorter than 550 nm in the ASOS visibility monitor (515 nm).

HAZE EPISODE STUDY

The strongest haze/ $\text{PM}_{2.5}$ episode in the two summer months of this study occurred on July 15–19, 1999 (Figure 2). A strong cold front crossed the mid-Atlantic region on July 10 and stalled to the south by July 12. Easterly winds in the wake of the front brought intermittent clouds and showers to the region until the front finally dissipated on July 14. Remarkably low $\text{PM}_{2.5}$ (~5 $\mu\text{g}/\text{m}^3$) was recorded during this period. Surface high pressure moved over the region on July 16 and remained in place until July 19. Daily mean temperatures of 28–30 °C were observed during this period. Fine particles began to accumulate on July 15 and reached maximum concentrations on July 19. Figure 7 shows the 72-hr HY-SPLIT back trajectories initiated at 1000 m (900 hPa) above FME at 1:00 p.m. (EST) every day between July 14–July 20, 1999. Trajectory heights of 1000 m were chosen for a few reasons. First, accuracy of back trajectories increases with height above ground level because the model is unable to fully resolve near surface frictional and turbulent effects. In addition, complex terrain in the mid-Atlantic, with peaks in the Appalachian Mountains exceeding 1000 m, can further decrease near surface accuracy. Second, a strong nocturnal inversion develops nightly in quiescent summer conditions, and major transport of pollutants often occurs above the inversion layer.

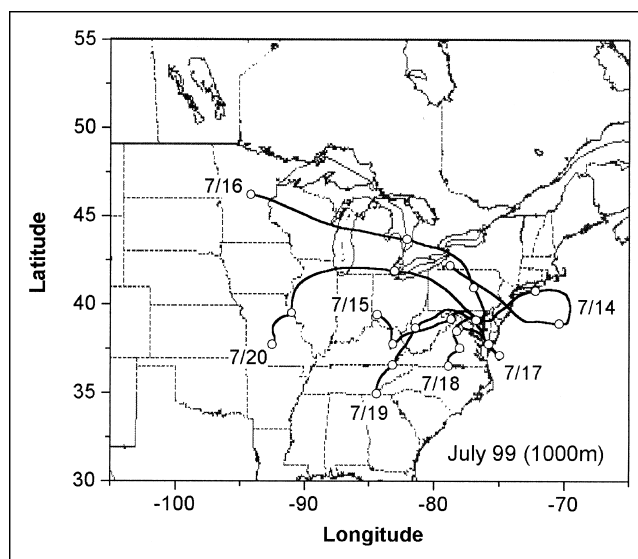


Figure 7. Three-day air parcel back trajectories initiating at 1000 m above FME at 1:00 p.m. EST for July 14–20, 1999. The circles indicate 24-hr intervals.

From July 14 to July 19, SO_4^{2-} concentrations at FME increased 3-fold from ~5 to ~18 $\mu\text{g}/\text{m}^3$ while carbonaceous material increased from ~4 to ~6 $\mu\text{g}/\text{m}^3$. The accumulation in the $\text{PM}_{2.5}$ mass was therefore primarily caused by ammoniated sulfate.

Hourly $\text{PM}_{2.5}$ mass (TEOM) and CO concentrations are shown with temperature and RH in Figure 8. The typical diurnal cycle for RH and temperature appears from July 16 to 18 with maximum temperatures >32 °C and RH ranging between 50 and 90%. CO, with its long atmospheric lifetime, is a good tracer for combustion. In the urban environment, CO concentrations are largely controlled by motor-vehicle emissions and boundary layer dispersion.^{11,42} The CO peaks in the early morning hours are caused by intensive emissions from rush-hour traffic into the shallow morning PBL. CO concentrations reach a minimum in the early afternoon hours because of vertical dispersion into a deeper PBL. CO then gradually accumulates in the NBL. The weaker morning CO peaks on July 17 and 18 are caused by lower weekend traffic volume.

Above the surface, nocturnal low-level jets (LLJ), centered at ~500 m AGL with a maximum wind speed of more than 10 m/sec, were observed by the FME radar profiler during the nights of July 16–July 17 and July 17–July 18 (see www.meto.umd.edu/~ryan/summary99.htm).⁴³ The LLJ of the type observed during this episode is a coastal plain phenomenon driven by differential heating across an upward sloping terrain.⁴⁴ In this episode, the LLJs formed at ~1900 EST and persisted until 0600–0700 EST. The LLJ diminished during the night of July 18–19, resulting in a relatively calm condition that partly explained the higher nighttime CO concentration. The

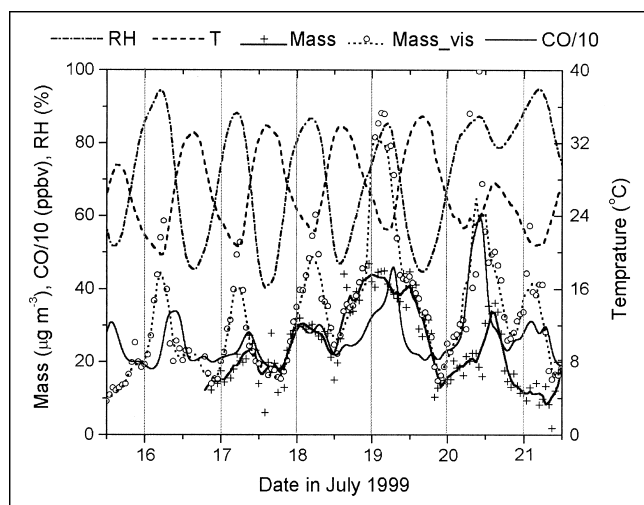


Figure 8. Time series of 1-hr $PM_{2.5}$ mass (TEOM) and CO along with temperature and RH at FME between July 15 and 21, 1999. $Mass_{vis}$ indicates the effective aerosol mass with respect to light extinction (see text). The lines associated with mass and $mass_{vis}$ indicate the 4-hr moving averages.

arrival of a cold front late on July 19 brought stronger winds, a cleaner air mass, and lower CO concentrations.

$PM_{2.5}$ concentrations respond more strongly to long-range transport effects than CO because of its predominantly SO_4^{2-} content. Back trajectories show easterly transport on July 14 shifting gradually to the northwest by July 16. Sulfate concentrations increased significantly on July 15 as the prevailing transport direction became westerly. While westerly winds continued in the near surface layers, a weak mesoscale recirculation that developed east of Cape Hatteras pushed southeasterly winds into the region. Back trajectories show slow southeasterly flows aloft throughout July 17 and persisting to midday on July 18 (Figure 7). The diurnal variation of $PM_{2.5}$ in the presence of this wind shear regime is similar to CO, with maximum concentrations at night falling off in the afternoon hours (Figure 8). This diurnal pattern is explained by the rising PBL in the afternoon entraining air from the cleaner southeasterly flow. The recirculation, in contrast, prevented quick dissipation of pollutants. Reflecting the complexity of this scenario, SO_4^{2-} concentration only increased moderately on July 16–17.

By midday on July 18, the upper level disturbance and associated vertical wind shear had dissipated. As prevailing winds returned westerly, $PM_{2.5}$ concentrations increased more rapidly than did CO concentrations. By noon on July 19, $PM_{2.5}$ reached its episode maximum, $\sim 45 \mu\text{g}/\text{m}^3$. Since the afternoon of July 19, convection developed across the mid-Atlantic region in advance of a north-to-south moving cold front. The radar profiler shows a shift to strong north-northeasterly winds late on July 19 becoming easterly as the frontal boundary passed

between 0100 and 0700 EST on July 20. By 0001 EST on July 20, $PM_{2.5}$ concentration was down to $\sim 15 \mu\text{g}/\text{m}^3$.

Effective aerosol mass per unit volume with respect to light extinction ($mass_{vis}$) at an hourly resolution was estimated from the measured b_{ext} . A mass extinction efficiency of $7.6 \text{ m}^2/\text{g}$ (from Figure 6) was used to convert b_{ext} to $mass_{vis}$ [i.e., $mass_{vis} (\mu\text{g}/\text{m}^3) = b_{ext}/7.6 \text{ m}^2/\text{g}$]. The $mass_{vis}$ was clearly influenced by both RH and $PM_{2.5}$ mass (Figure 8). During the July 15–July 19 episode, the highest RH $\sim 90\%$ occurred at each early morning with the lowest ambient temperature. The $mass_{vis}$ agreed with the dry $PM_{2.5}$ mass (from TEOM) very well for RH $< 60\%$, suggesting that the mass extinction efficiency of $7.6 \text{ m}^2/\text{g}$, estimated from 24-hr b_{ext} , reconstructed $PM_{2.5}$ mass, and calculated water, can be appropriate for this case. The high RH period during the nights of July 17–July 18 and July 18–July 19 agree with the aerosol accumulation closely in time, and this resulted in visibility reduction at night to $\sim 5 \text{ km}$. The cold front moving into this area on July 20 lowered ambient temperature, increased RH, and brought light rain in the morning hours (0641–1005 EST) of July 20. At noon of July 20, the high RH enhanced the b_{ext} caused by dry aerosol by as much as a factor of 3 (Figure 8).

CONCLUSIONS

Haze is well understood as a result of light-scattering by small particles in the atmosphere. However, the evolution of a haze episode is complicated, involving the formation, growth, transport, and dispersion of aerosols. This paper investigates the general features of summertime $PM_{2.5}$ in the mid-Atlantic region. Based on the measurements by various techniques (SFS, FRM, TEOM) at FME, July 1999, which was warmer and drier than July 2000, appeared to have a mean $PM_{2.5}$ mass concentration $\sim 35\%$ higher than that of July 2000. The mass fraction of ammoniated sulfate gradually increased to $\sim 60\%$ for $PM_{2.5} > 30 \mu\text{g}/\text{m}^3$ while the mass fraction of carbonaceous material decreased to $\sim 20\%$. Ammoniated sulfate was most responsible for summertime haze at this locale. By comparing the FME data with the IMPROVE network, high SO_4^{2-} concentrations can appear both upwind and downwind of FME. Widespread SO_4^{2-} , over a region $\sim 400 \text{ km}$ in diameter, compared with a much narrower distribution of carbonaceous material around the B-W corridor, implies that the source of SO_4^{2-} is not local. Therefore, long-range transport of SO_4^{2-} from its source region, likely the U.S. Midwest, is crucial for haze formation over the mid-Atlantic region.

The pollutant concentration depends not only on its sources but also on sinks, which usually includes dispersion and deposition. A stationary high-pressure system that produces clear sky, subsidence, and relatively

stagnant conditions can lead to accumulation of pollutants. The most serious haze/PM_{2.5} episode during the two summer months occurred July 15–19, 1999, and was associated with a persistent ridge of high pressure. The 24-hr PM_{2.5} concentration monotonically increased from 12 to 35 µg/m³ over 5 days. Back trajectory analysis suggests that westerly transport with some periods of recirculation occurred during this episode. The PM_{2.5} concentration reached its maximum during the night of July 18–19 in the calmest nighttime PBL without the influence of nocturnal LLJs.

Relative humidity is shown to be another important factor influencing haze formation. Aerosol water content in ambient conditions was estimated based on thermodynamic equilibrium. A good correlation is achieved between hydrated PM_{2.5} mass and extinction coefficient b_{ext} leading to an aerosol mass extinction efficiency of $7.6 \pm 1.7 \text{ m}^2/\text{g}$. At the peak of the July 15–19 haze episode, water likely contributed to ~40% of the light extinction. Lowest visibility usually occurs at night because of higher RH. A meteorological pattern that allows simultaneous accumulation of PM_{2.5} and water vapor is critical in the summertime haze formation and should warrant further experimental and modeling studies.

ACKNOWLEDGMENTS

This work was supported in part by Baltimore Gas and Electric Co. and Potomac Electric Power Co. through EPRI and Maryland Industrial Partnerships, with additional support through the EPA under grant number R826731476. The authors thank the Maryland Department of the Environment for additional support at the sampling site. Tad Aburn, William Butler, Ed Gluth, Steven Kohl, Fran Pluciennik, Dave Preece, John Quinn, and Charles Piety provided substantive assistance. The authors also thank Athanasios Nenes for providing the ISORROPIA model and William Malm and John Watson for useful discussions. Reviewers' comments are appreciated.

REFERENCES

1. Watson, J.G. Visibility: Science and Regulation; *J. Air & Waste Manage. Assoc.* **2002**, *52*, 628-713.
2. Chu, R. *Algorithms for the Automated Surface Observing System (ASOS)*; ISL Office Note 94-4; NWS/OSD: Silver Spring, MD, 1994; p 106.
3. Malm, W.C.; Sisler, J.F.; Huffman, D.; Eldred, R.A.; Cahill, R.A. Spatial and Seasonal Trends in Particle Concentration and Optical Extinction in the United States; *J. Geophys. Res.* **1994**, *99* (D1), 1347-1370.
4. *Spatial and Seasonal Patterns and Temporal Variability of Haze and its Constituents in the United States: Report III*; Interagency Monitoring of Protected Visual Environments (IMPROVE): Fort Collins, CO, 2000.
5. Finlayson-Pitts, B.J.; Pitts, J.N. *Chemistry of the Upper and Lower Atmosphere*; Academic Press: San Diego, CA, 1999; p 369.
6. Malm, W.C.; Molenar, J.V.; Eldred, R.A.; Sisler, J.F. Examining the Relationship among Atmospheric Aerosols and Light Scattering and Extinction in the Grand Canyon Area; *J. Geophys. Res.* **1996**, *101* (D14), 19251-19266.
7. Ryan, W.F.; Doddridge, B.G.; Dickerson, R.R.; Morales, R.M.; Hallock-Waters, K.A.; Roberts, P.T.; Blumenthal, D.L.; Anderson, J.A.; Civerolo, K.L. Pollutant Transport during a Regional O₃ Episode in the Mid-Atlantic States; *J. Air & Waste Manage. Assoc.* **1998**, *48*, 786-797.
8. Russell, P.B.; Hobbs, P.V.; Stowe, L.L. Aerosol Properties and Radiative Effects in the United States East Coast Haze Plume: An Overview of the Tropospheric Aerosol Radiative Forcing Observational Experiment (TRAFIX); *J. Geophys. Res.* **1999**, *104* (D2), 2213-2222.
9. Malm, W.C. Characteristics and Origins of Haze in the Continental United States; *Earth-Sci. Rev.* **1992**, *33*, 1-36.
10. Stehr, J.W.; Dickerson, R.R.; Hallock-Waters, K.A.; Doddridge, B.G.; Kirk, D. Observation of NO_y, CO, and SO₂ and the Origin of Reactive Nitrogen in the Eastern United States. *J. Geophys. Res.* **2000**, *105* (D3), 3553-3563.
11. Chen, L.-W.A.; Doddridge, B.G.; Dickerson, R.R.; Muller, P.K.; Chow, J.C.; Butler, W.A.; Quinn, J. Seasonal Variations in Elemental Carbon Aerosol, Carbon Monoxide, and Sulfur Dioxide: Implications for Sources; *Geophys. Res. Lett.* **2001**, *28* (9), 1711-1714.
12. Chen, L.-W.A.; Doddridge, B.G.; Dickerson, R.R.; Chow, J.C.; Henry, R.C. Origins of Fine Aerosol Mass in the Baltimore-Washington Corridor: Implications from Observations, Factor Analysis, and Ensemble Air Parcel Back Trajectories; *Atmos. Environ.* **2002**, *36* (28), 4541-4554.
13. Chen, L.-W.A. Ph.D. Dissertation, University of Maryland, College Park, August 2002.
14. Chow, J.C.; Watson, J.G.; Fujita, E.M.; Lu, Z.; Lawson, D.R. Temporal and Spatial Variations of PM_{2.5} and PM₁₀ Aerosol in the Southern California Air Quality Study; *Atmos. Environ.* **1994**, *28*, 2061-2080.
15. Chow, J.C.; Watson, J.G.; Zhiqiang, L.; Lowenthal, D.H.; Frazier, C.A.; Solomon, P.A.; Thuillier, R.H.; Magliano, K. Descriptive Analysis of PM_{2.5} and PM₁₀ at Regionally Representative Locations during SJAQAS/AUSPEX; *Atmos. Environ.* **1996**, *30*, 2079-2112.
16. Chow, J.C.; Waston, J.G.; Pritchett, L.C.; Pierson, W.R.; Frazier, C.A.; Purcell, R.G. The DRI Thermal/Optical Reflectance Carbon Analysis System: Description, Evaluation and Applications in U.S. Air Quality Studies; *Atmos. Environ.* **1993**, *27*, 1185-1201.
17. Chow, J.C.; Watson, J.G.; Crow, D.; Lowenthal, D.H.; Merrifield, T. Comparison of IMPROVE and NIOSH Carbon Measurements; *Aerosol Sci. Technol.* **2001**, *34* (1), 1-12.
18. Watson, J.G.; Lioy, P.J.; Mueller, P.K. The Measurement Process: Precision, Accuracy, and Validity. In *Air Sampling Instruments for Evaluation of Atmospheric Contaminants*, 8th ed.; Cohen, B., Hering, S.V., Eds.; American Conference of Governmental Industrial Hygienists: Cincinnati, OH, 1995; pp L2-L8.
19. Dickerson, R.R.; Delany, A.C. Modification of a Commercial Gas Filter Correlation CO Detector for Increased Sensitivity; *J. Atmos. Oceanic Technol.* **1988**, *5* (3), 424-431.
20. Doddridge, B.G.; Dickerson, R.R.; Spain, T.G.; Oltmans, S.J.; Novelli, P.C. Carbon Monoxide Measurements at Mace Head, Ireland. In *Ozone in the Troposphere and Stratosphere*; Hudson, R.D., Ed.; NASA: Washington, DC, 1994; NASA Conf. Publ. 3266, p 134-137.
21. Draxler, R.R. *Hybrid Single-Particle Lagrangian Integrated Trajectories (HY-SPLIT): Model Description*; Tech. Memo; ERL ARL-166; NOAA: Washington, DC, 1998; p 23.
22. Draxler, R.R. The Accuracy of Trajectories during ANATEX Calculated Using Dynamic Model Analysis versus Rawinsonde Observations; *J. Appl. Meteorol.* **1991**, *30*, 1466-1467.
23. Watson, J.G.; Chow, J.C. Comparison and Evaluation of In Situ and Filter Carbon Measurements at the Fresno Supersite; *J. Geophys. Res.* **2002**, *107* (D21), 8341-8355.
24. Cyrus, J.; Dietrich, G.; Kreyling, W.; Tuch, T.; Heinrich, J. PM_{2.5} Measurements in Ambient Aerosol: Comparison between Harvard Impactor (HI) and the Tapered Element Oscillating Microbalance (TEOM) System. *Sci. Total Environ.* **2001**, *278* (1-3), 191-197.
25. White, W.H.; Roberts, P.T. On the Nature and Origins of Visibility-Reducing Aerosols in the Los Angeles Air Basin; *Atmos. Environ.* **1977**, *11*, 803-812.
26. Seinfeld, J.H.; Pandis, S.N. *Atmospheric Chemistry and Physics*; Wiley & Sons: New York, 1998; p 533.
27. Turpin, B.J.; Lim, H.-J. Species Contributions to PM_{2.5} Mass Concentrations: Revising Common Assumptions for Estimating Organic Mass; *Aerosol Sci. Technol.* **2001**, *35*, 602-610.
28. Rees, S.L.; Takahama, S.; Robinson, A.L.; Khlystov, A.; Pandis, S.N. Seasonal Composition of PM_{2.5} and Performance of the Federal Reference Method in Pittsburgh. In *PM_{2.5} and Electric Power Generation: Recent Findings and Implications*; Summaries of a Conference Sponsored by National Energy Technology Laboratory: Pittsburgh, PA, 2002; p 69-70.
29. Richardson, C.B.; Spann, J.F. Measurement of the Water Cycle in a Levitated Ammonium Sulfate Particle; *J. Aerosol Sci.* **1984**, *15*, 563-571.
30. Poulida, O.; Dickerson, R.R.; Doddridge, B.G.; Holland, J.Z.; Wardell, R.G.; Watkins, J.G. Trace Gas Concentrations and Meteorology in Rural Virginia: 1. Ozone and Carbon Monoxide; *J. Geophys. Res.* **1991**, *96* (D12), 22461-22475.
31. Hallock-Waters, K.A.; Doddridge, B.G.; Dickerson, R.R.; Spitzer, S.; Ray, J.D. Carbon Monoxide in the U.S. Mid-Atlantic Troposphere: Evidence for a Decreasing Trend; *Geophys. Res. Lett.* **1999**, *26*, 2861-2864.

32. Moy, L.A.; Dickerson, R.R.; Ryan, W.F. How Meteorological Conditions Affect Tropospheric Trace Gas Concentrations in Rural Virginia; *Atmos. Environ.* **1994**, *28*, 2789-2800.
33. *National Air Pollutants Emission Trends Report, 1990-1994*; EPA/454/R-95/011; U.S. Environment Protection Agency: Washington, DC, 1995.
34. Prospero, J.M. Long-Term Measurements of the Transport of African Mineral Dust to the Southeastern United States: Implications for Regional Air Quality. *J. Geophys. Res.* **1999**, *104* (D13), 15,917-15,927.
35. Air Parcel Back Trajectory Analysis for 7/3/1999 Crustal Episode in the Southeastern United States. Available at: <http://www.atmos.umd.edu/~bruce/MARCH-Atl.html> (accessed June 2003), link: Chen et al. 2003 paper supplementary material.
36. Nenes, A.; Pilinis, C.; Pandis, S.N. ISORROPIA. A New Thermodynamic Model for Multiphase Multicomponent Inorganic Aerosols; *Aquatic Geochem.* **1998**, *4*, 123-152.
37. Nenes, A.; Pilinis, C.; Pandis, S.N. Continued Development and Testing of a New Thermodynamic Aerosol Module for Urban and Regional Air Quality Models; *Atmos. Environ.* **1999**, *33*, 1553-1560.
38. Tang, I.N.; Munkelwitz, H.R. Composition and Temperature Dependence of the Deliquescence Properties of Hygroscopic Aerosols; *Atmos. Environ.* **1993**, *27A*, 467-473.
39. Malm, W.C.; Day, D.E. Estimates of Aerosol Species Scattering Characteristics as a Function of Relative Humidity; *Atmos. Environ.* **2001**, *35*, 2845-2860.
40. Hegg, D.A.; Livingston, J.; Hobbs, P.V.; Novakov, T.; Russell, P. Chemical Apportionment of Aerosol Column Optical Depth off the Mid-Atlantic Coast of the United States; *J. Geophys. Res.* **1997**, *102* (D21), 25293-25303.
41. Seinfeld, J.H.; Pandis, S.N. *Atmospheric Chemistry and Physics*; Wiley & Sons: New York, 1998; p 1132.
42. Glen, W.G.; Zelenka, M.P.; Graham, R.C. Relating Meteorological Variables and Trends in Motor Vehicle Emissions to Monthly Urban Carbon Monoxide Concentrations; *Atmos. Environ.* **1996**, *30* (24), 4225-4232.
43. Radar Profiler Observations at FME for 7/17/1999-7/20/1999. Available at: <http://www.meto.umd.edu/~ryan/summary99.htm> (accessed June 2003).
44. Zhang, K.; Mao, H.; Civerolo, K.; Berman, S.; Ku, J.-Y.; Rao, S.T.; Doddridge, B.G.; Philbrick, R.C.; Clark, R. Numerical Investigation of Boundary-Layer Evolution and Nocturnal Low-Level Jets: Local versus Non-Local PBL Schemes; *Environ. Fluid Mech.* **2001**, *1*, 171-208.

About the Authors

Dr. L.-W. Antony Chen is a research associate and Dr. Judith C. Chow is a research professor at the Desert Research Institute in Reno, NV. Dr. Bruce G. Doddridge is an associate research professor and Dr. Russell R. Dickerson is a professor of meteorology at the University of Maryland in College Park, MD. William F. Ryan is a research meteorologist at Pennsylvania State University in University Park, PA. Dr. Peter K. Mueller is the principal of TropoChem in Palo Alto, CA. Address correspondence to: Dr. L.-W. Antony Chen, Desert Research Institute, University and Community College System of Nevada, 2215 Raggio Parkway, Reno, NV 89512; e-mail: antony@dri.edu.